Optical Materials 75 (2018) 501–507

Contents lists available at ScienceDirect

Optical Materials

journal homepage: www.elsevier.com/locate/optmat

Towards metal chalcogenide nanowire-based colour-sensitive photodetectors

Edgars Butanovs*, Jelena Butikova, Aleksejs Zolotarjovs, Boris Polyakov

Institute of Solid State Physics, University of Latvia, Kengaraga Street 8, Riga, LV-1063, Latvia

ARTICLE INFO

Article history:
Received 21 August 2017
Received in revised form
20 October 2017
Accepted 6 November 2017

Keywords:
PbS
In_2S_3
CdS
ZnSe
Nanowire
Photodetector

ABSTRACT

In recent years, nanowires have been shown to exhibit high photosensitivities, and, therefore are of interest in a variety of optoelectronic applications, for example, colour-sensitive photodetectors. In this study, we fabricated two-terminal PbS, In_2S_3, CdS and ZnSe single-nanowire photoresistor devices and tested applicability of these materials under the same conditions for colour-sensitive (405 nm, 532 nm and 660 nm) light detection. Nanowires were grown via atmospheric pressure chemical vapour transport method, their structure and morphology were characterized by scanning and transmission electron microscopy (SEM and TEM), X-ray diffraction (XRD), and optical properties were investigated with photoluminescence (PL) measurements. Single-nanowire photoresistors were fabricated via *in situ* nanomanipulations inside SEM, using focused ion beam (FIB) cutting and electron-beam-assisted platinum welding; their current-voltage characteristics and photoresponse values were measured. Applicability of the tested nanowire materials for colour-sensitive light detection is discussed.

1. Introduction

Colour-sensitive photodetectors are desirable for a large variety of applications, for instance, in optical communications, digital imaging and environmental monitoring [1–4]. In recent years, nanowires (NWs) have been demonstrated to be superior to their bulk counterparts as photodetector materials mainly due to their higher sensitivities, which arise from the NW high surface area/volume ratio resulting in high density of surface states that act as trap sites for photogenerated holes, therefore increasing electron lifetime and enhancing the photocurrent [5,6]. Semiconducting chalcogenide materials with direct bandgap and large absorption coefficients, such as PbS, In_2S_3, CdS, ZnSe, are great candidates for next-generation NW-based light detectors due to their excellent photodetection properties [6–9]. Typical photodetectors can detect only a specific spectral band, therefore are not suitable for multi-colour detection with spectral selectivity. There are two general approaches of making colour-sensitive detectors: using broad-spectrum materials and wavelength-selective filters, or combining several materials with different bandgaps, including material doping and composition tuning. Using broad-spectrum photodetector materials combined with absorptive colour filters is a possibility; however, it involves additional fabrication steps and, to obtain highest efficiency, one would prefer light to be converted to photocurrent rather than reflected or absorbed in the filter layer. Research has been done on compositionally tuneable NWs and doping of NWs for wavelength-selective light detection [10,11], but there is a difficulty to extend the optical band outside the visible light range. Furthermore, it has been demonstrated that colour imaging is possible by varying the radius of silicon NWs to control spectral sensitivities [12]. However, a versatile strategy to obtain spectral selectivity is to select arbitrary photosensitive material NWs with different bandgaps, and incorporate them in a composite thin film or on an insulating substrate. Liu et al. demonstrated a method of incorporating photosensitive CdS, CdSeS and CdSe NWs into an amorphous indium zinc oxide thin film to obtain a transparent thin-film-transistor array, showing that such concept could be possibly used to fabricate multi-colour photodetectors [13]. Sang et al. utilized CdS, SnO_2, ZnO and Ga_2O_3 one-dimensional nanostructures to demonstrate colour-sensitive photodetection by simultaneously integrating them into an insulating substrate with a two-terminal device structure [14]. In such a way, the cut-off wavelengths of the selected semiconductor NW materials, defined by the bandgap, will determine the spectral selectivity. This approach benefits from substantial freedom to choose NW materials with desirable spectral band and high

* Corresponding author.
E-mail address: edgarsb@cfi.lu.lv (E. Butanovs).

https://doi.org/10.1016/j.optmat.2017.11.010
0925-3467/

photoresponse. Furthermore, large-scale printing of NWs at defined locations on flexible substrates via roll-to-roll transfer has been demonstrated [15], thus enabling the development of NW based all-printed electronic and optoelectronic devices at low cost and with high performance.

In this work, we synthesised PbS, In_2S_3, CdS and ZnSe NWs and fabricated single-nanowire two-terminal photoresistor devices to test the applicability of these materials for colour-sensitive (red, green and blue light) photodetector applications, if they would be simultaneously incorporated on the same substrate. It is important to note that all these devices were prepared using the same method and tested under the same conditions. The measured NW photodetector properties were compared and analysed.

2. Experimental details

2.1. Nanowire synthesis and characterization

The following material NWs were synthesised via atmospheric pressure chemical vapour transport method in a horizontal quartz tube reactor by adjusting previously reported growth parameters: PbS [16], In_2S_3 [17], CdS [18], and ZnSe [19]. In all the cases, the NWs were grown on oxidized silicon wafers Si(110)/SiO_2 (*Semiconductor Wafer, Inc.*) coated with spherical Au nanoparticles used as a catalyst (*Smart materials*, water suspension, 50 nm diameter).

PbS NWs: 0.25 g $PbCl_2$ powder (*98%, Sigma Aldrich*) was loaded in a ceramic boat and placed in the centre of the quartz tube at 650 °C, Au/Si substrate was placed downstream in a lower temperature region. Excessive amount of sulphur powder (*enola SIA*) was placed upstream at 250 °C to create sulphur-rich atmosphere, while N_2 was used as a carrier gas. The temperature was kept constant for 20 min, followed by natural cooling to room temperature.

In_2S_3 NWs: Mixture of 0.5 g In and 0.5 g $InCl_3$ (*98%, Sigma-Aldrich*) powders were used as a source material and sent to the centre of the quartz tube. Au/Si substrate and sulphur powder were placed downstream and upstream, respectively, as in the previous case. Ar/H_2 (5%) gas mixture was used as a vapour carrier. The furnace was heated to 800 °C, temperature was held constant for

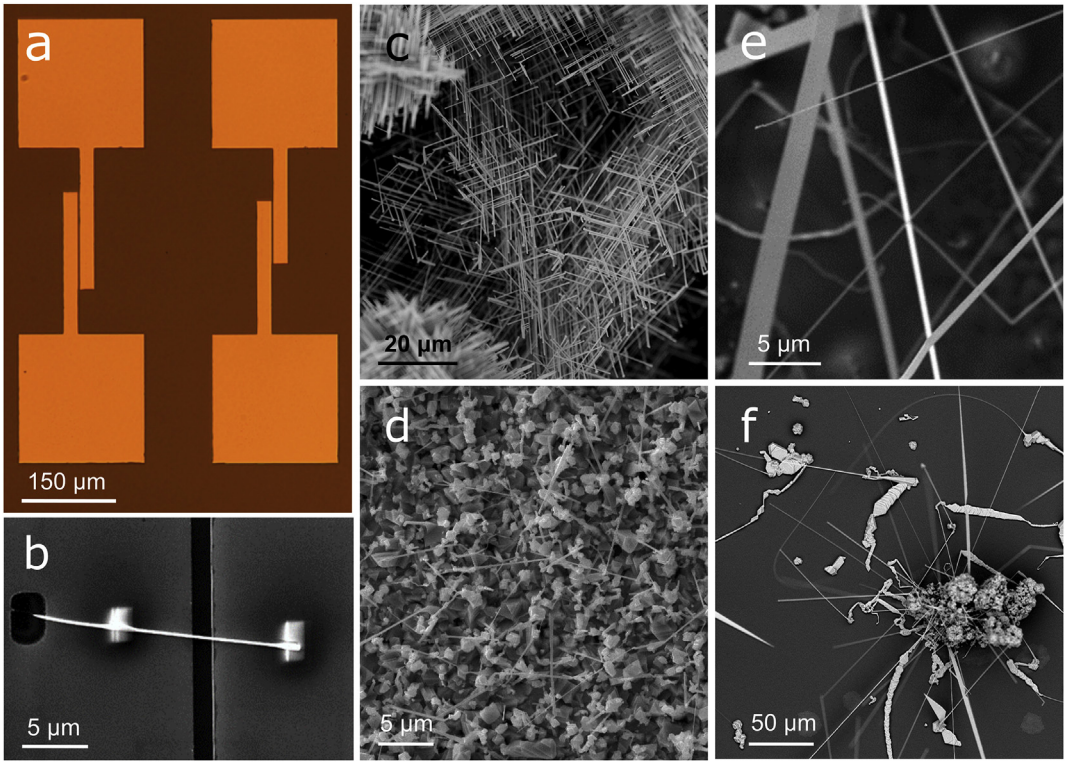

Fig. 1. (a) Optical microscope image of gold microelectrodes on the oxidized silicon substrate; SEM images of (b) a typical as-prepared nanowire photoresistor; as-grown (c) PbS, (d) In_2S_3, (e) CdS and (f) ZnSe nanowires.

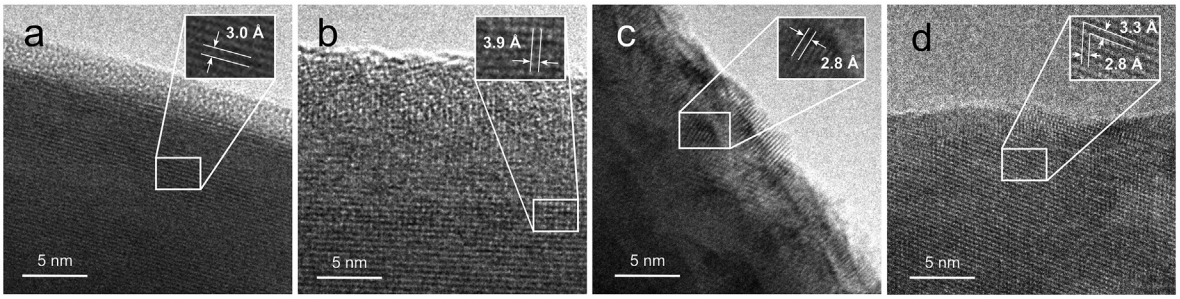

Fig. 2. TEM images of (a) PbS, (b) In_2S_3, (c) CdS and (d) ZnSe nanowires. Insets show measured atomic interlayer distances.

45 min and then was let to cool down naturally to room temperature.

CdS NWs: CdS powder (*98%, Alfa Aesar*) was thermally evaporated in a quartz tube at 950 °C temperature for 30 min, followed by a natural cooling. The vapour was carried downstream to the Au/Si substrate by N_2 gas.

ZnSe NWs: 0.2 g home-made ZnSe powder was placed at the centre of the quartz tube and evaporated at 1000 °C for 2.5 h, using Ar/H_2 (5%) gas to carry vapour downstream to the Au/Si substrate at a lower temperature region, and then cooled down naturally to the room temperature.

As-prepared NW morphology was characterized by scanning electron microscopy (SEM, Lyra, Tescan), whereas the inner crystalline structure was revealed by transmission electron microscopy (TEM, Tecnai GF20, FEI) using the operating voltage of 200 kV. X-ray diffraction (XRD, PANalytical, X'Pert Pro Powder) was carried out by monochromatic Cu Kα irradiation to confirm the material and the phase of a NW. Room-temperature photoluminescence (PL, Hamamatsu R92P PMT) spectra with the excitation wavelength of 266 nm (fourth harmonic of Nd:YAG laser) for all NWs and infrared (IR) absorption spectrum (Bruker Equinox 55 FT-IR Spectrometer) for PbS NWs were measured to investigate their optical properties.

2.2. Single nanowire photoresistor fabrication

Firstly, gold microelectrodes with the gap width of 2 μm were prepared on an oxidized silicon wafer by conventional photolithography technique (see Fig. 1(a)). Briefly, microelectrode pattern was obtained using direct write laser lithography (μPG 101, Heidelberg Instruments) on SU-8 2003 photoresist (MicroChem), 5/45 nm Cr/Au film was deposited via thermal evaporation method, followed by a *lift-off* procedure.

Secondly, single NW photoresistors were fabricated using *in situ* nanomanipulations inside SEM-FIB. As-grown NWs were mechanically transferred from the Si substrate to the as-prepared gold microelectrodes by welding a single NW to the tungsten (W) nanomanipulator probe using electron-beam-assisted platinum (Pt) deposition. After aligning and placing it on top of the microelectrodes, NW was cut off from the W probe with gallium (Ga) ion beam and welded to the electrodes with Pt deposition to ensure the electric contact and fixed position. SEM image of a typical as-prepared photoresistor is displayed in Fig. 1(b), where the narrow dark strip is the gap between the electrodes, two small rectangles on the NW are the deposited Pt contacts, and the trench appeared due to the cutting NW by ion beam milling.

2.3. Device measurements

Current-voltage (I_{ds}-V_{ds}) characteristics and photoresponse of the fabricated two-terminal devices were measured at zero gate voltage ($V_g = 0$ V) with a two-contact micro probe station connected with Model 6485 Keithley Picoammeter, Model 2000 Keithley Multimeter and a voltage source (33220A Waveform Generator, Agilent). 405 nm, 532 nm and 660 nm wavelength semiconductor diode lasers with light intensity of 2 W/cm^2 were used as an illumination source for the photoresponse measurements. All measurements were carried out in air and at room temperature.

3. Results and discussion

3.1. Morphology, structure and PL measurements

SEM was used to image as-grown NW arrays (see Fig. 1(c–f)) and to determine the size of individual NWs. The length varied from 20 to 30 μm for PbS and In_2S_3 NWs to several hundred micrometres for CdS and ZnSe NWs. The diameter of NWs was in the range of 50–300 nm. The Au catalyst nanoparticles were observed on the top end of In_2S_3, CdS and ZnSe NWs, which indicates Vapour-Liquid-Solid (VLS) growth, as was expected [20–22]; however, that was not the case for PbS NWs: these NWs exhibited growth in hierarchical, orthogonally branched clusters, as reported previously [23]. It is worth noting that nanobelts were also observed on as-prepared CdS and ZnSe samples, along with the NWs, though only NWs were used to fabricate photoresistor

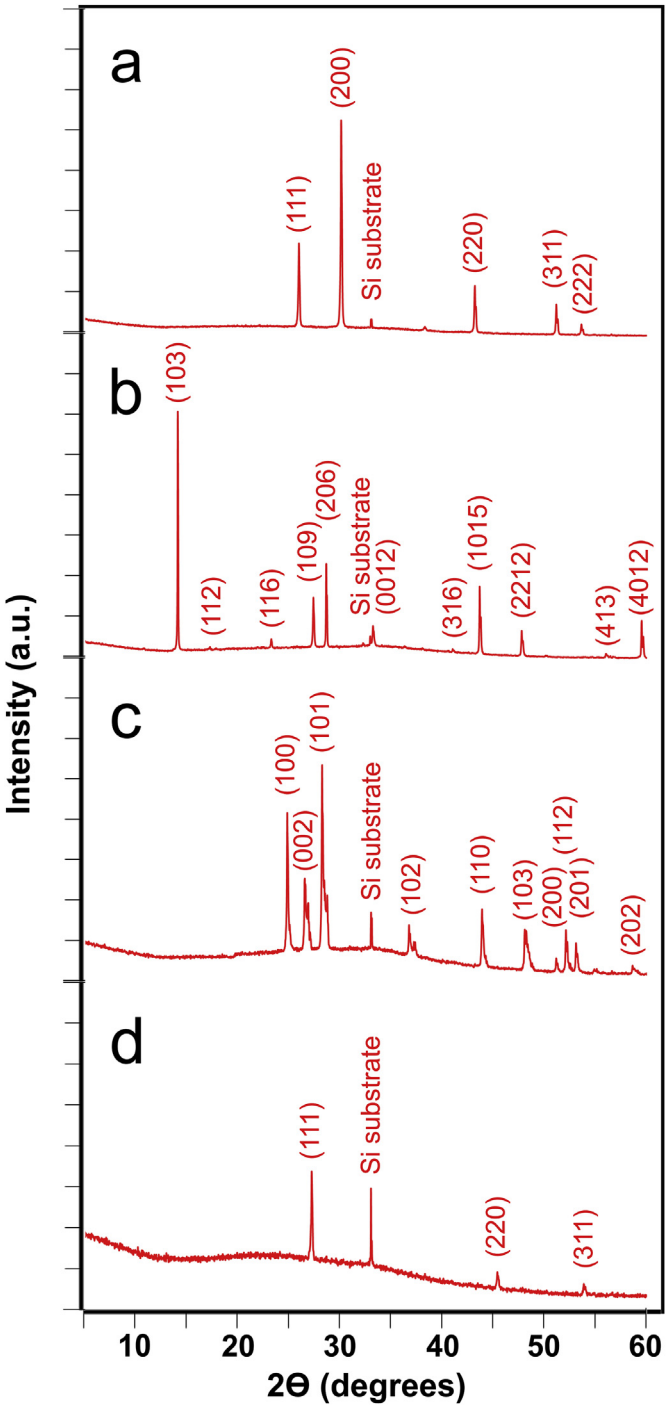

Fig. 3. XRD spectra of (a) PbS, (b) In_2S_3, (c) CdS and (d) ZnSe nanowire arrays on a silicon substrate.

devices.

TEM investigations revealed inner crystalline structure of the NWs. Fig. 2(a) shows highly crystalline nature of a PbS NW. Resolved atomic planes are separated by a distance of 3.0 Å, which corresponds to (200) planar spacing of a cubic (rock-salt) PbS crystal (a = 5.94 Å [24]). Similarly, an In_2S_3 NW exhibited high crystallinity, as can be seen in Fig. 2(b). Interplanar spacing was measured to be 3.9 Å, which is in a good agreement with the lattice constant of tetragonal β-In_2S_3 (a = 7.8 Å [25]). Polycrystalline shell was observed around the CdS NW, which is visible in Fig. 2(c). According to interplanar distance measurements, such crystallites have cubic (zinc blende) structure with planar spacing of 2.7–2.8 Å, which corresponds to the lattice constant value a = 5.45 Å [26]. As can be seen in Fig. 2(d), the distances between adjacent ZnSe lattice planes was measured to be 3.3 Å and 2.8 Å, which corresponds to cubic (zinc blende) structure (a = 5.6 Å [27]).

Fig. 3 depicts the XRD patterns of the as-grown NW arrays, which verifies their material and phase. The diffraction peaks in PbS NW XRD pattern were indexed to a cubic PbS crystal [24], In_2S_3 NW pattern to a tetragonal β-In_2S_3 crystal [25], CdS NW pattern to a hexagonal wurtzite structure [28], and ZnSe XRD pattern was indexed to cubic (zinc blende) ZnSe crystal structure [27]. The peak at 33° is attributed to the diffraction in the Si substrate.

PL properties of the as-grown NWs were studied at the room temperature in the wavelength range from 380 nm to 580 nm, excited by 266 nm laser. Measured spectra are shown in Fig. 4. The bandgap of PbS NWs is around 0.4 eV and the optical absorption starts at 3100 nm, therefore luminescence band with maximum at 425 nm (see Fig. 4(a)) corresponds to higher energy band transitions [29,30]. Similar luminescence was measured on PbS nanocubes and thin films in other works by Cao et al. [31] and Tohidi et al. [32]. The inset of Fig. 4(a) depicts measured optical absorption spectrum of PbS NWs, thus confirming that the absorption starts around 3 μm wavelength light. Fig. 4(b, c, d) shows measured luminescence bands of In_2S_3, CdS and ZnSe, respectively. Their according maxima are 505 nm, 510 nm and 460 nm, that corresponds to bandgap values of 2.45 eV, 2.43 eV and 2.7 eV, in agreement with previous reports [6,19,20].

3.2. Device photoresponse measurements

Fig. 5 shows measured I_{ds}-V_{ds} curves of different as-prepared two-terminal NW devices. At least four photoresistors of each material were fabricated, so consistent conclusions could be made. Typically, nearly symmetrical characteristics were measured for all investigated NW materials, therefore indicating that ohmic contacts were formed between the electrodes and the NW. Features of non-linear quadratic ($I \sim V^2$) behaviour of the I-V curves may be interpreted as an effect of the space-charge limited current (SCLC), as other groups have previously shown in different material nanowires [33,34]. In addition, it is worth noting that as-fabricated devices exhibit high resistance, wherein, most probably, a considerable part arises due to a high contact resistance since performed NW characterization indicated highly crystalline structure. Possible causes of such increased resistance include high resistance of deposited Pt contacts due to a carbon presence from the metal-organic precursor [35].

Next, as-prepared NW device electrical response to an illumination of a light at different wavelengths was investigated. On-off photoresponse measurements, which are based on photoinduced conductivity changes, for three different illumination wavelengths at V_{ds} = 1 V bias of as-prepared NW photoresistor devices are

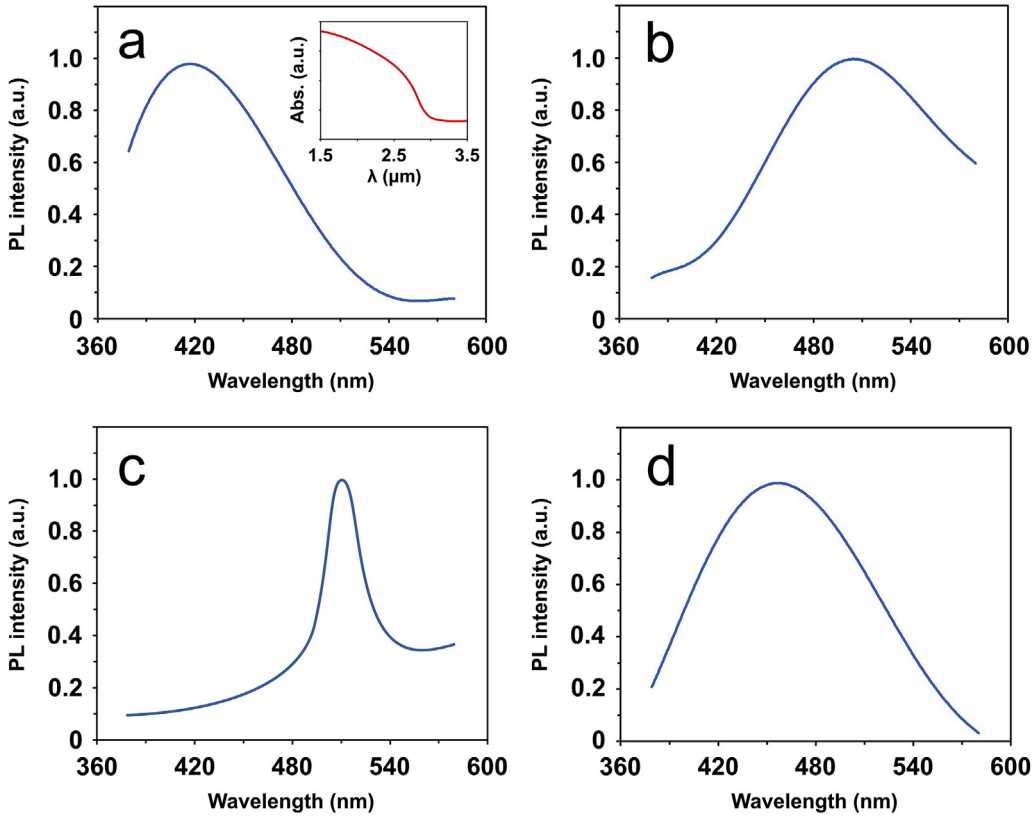

Fig. 4. Room-temperature PL spectra at the excitation wavelength of 266 nm of (a) PbS, (b) In_2S_3, (c) CdS and (d) ZnSe nanowire arrays on a silicon substrate. The inset shows the optical absorption in PbS NWs in 1.5–3.5 μm wavelength range.

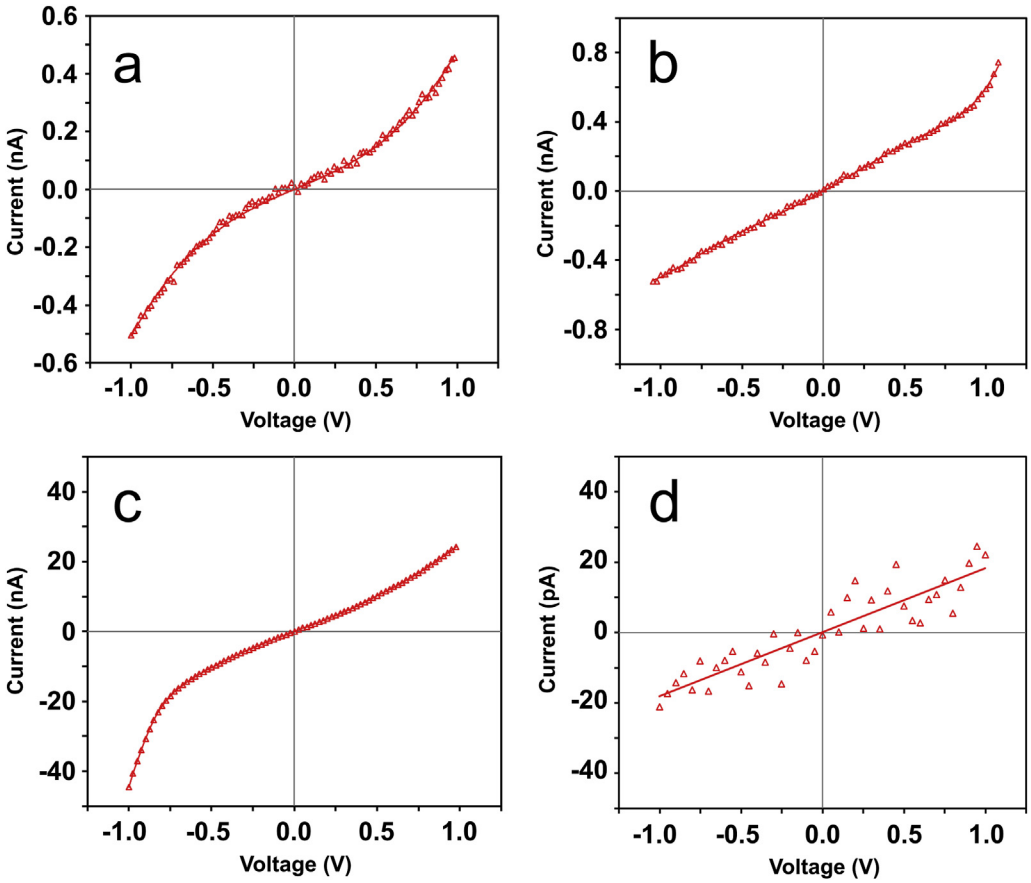

Fig. 5. Output (I_{ds}-V_{ds}) characteristics at $V_g = 0$ V of (a) PbS, (b) In_2S_3, (c) CdS and (d) ZnSe nanowire photoresistors.

depicted in Fig. 6. It can be seen that all four studied NW materials exhibit rapid (<1 s, in most cases) increase and decrease of the current after the illumination is turned on or off, respectively, except in the case of the In_2S_3 NW current decay time for 405 nm illumination, which features a second, slower time component, most probably do to a presence of trapping centres.

Table 1 shows the comparison of current enhancement ratios (I_{on}/I_{off}) of the studied NW materials in the context of their respective bandgap, which determines their cut-off wavelengths. Firstly, it can be seen that PbS NWs exhibit weak (I_{on}/I_{off} close to 1) photoresponse to all three illumination wavelengths; however, linear ratio vs. wavelength dependence was observed. Secondly, In_2S_3 and CdS NWs exhibit strong photoresponse to 405 nm illumination, and significantly weaker one to 532 nm and 660 nm illumination. Finally, ZnSe NWs show very strong response to 405 nm light, and no photoresponse was observed while illuminating them with 532 nm and 660 nm wavelength light. Obtained I_{on}/I_{off} value tendencies, for the most part, are as was anticipated from the material bandgap values; however, relatively weaker photoresponse to 660 nm illumination was expected for either CdS or In_2S_3 NWs.

Two important parameters for evaluating the quality of photoconductors are the current responsivity (R_λ) and the external quantum efficiency (EQE). R_λ and EQE are defined, respectively, as $R_\lambda = \Delta I/(PS)$ and $EQE = hcR_\lambda/(e\lambda)$ [36], where ΔI is the difference between the photocurrent I_{on} and the dark current I_{off}, P is the light power density, S is the effective illumination area (estimated as the electrode gap width × NW diameter), h is Planck's constant, c is the speed of light, e is the electron charge, and λ is the light wavelength. Large R_λ and EQE values correspond to a high photodetector sensitivity. Table 2 contains the calculated R_λ and EQE values of the studied NW devices. The obtained data shows a relatively wide range of values for different NW materials, however these values are comparable to other typical state-of-art 1D nanostructure photodetectors [37], thus indicating the potential to use such materials in future applications.

In principle, there are two approaches for determining the colour (red (660 nm), green (532 nm) or blue (405 nm)) of the incident light with such NW photoresistors, if they would be simultaneously incorporated on the same substrate as one optoelectronic device: by the wavelength cut-off due to the bandgap (signal or no signal) and by comparison of I_{on}/I_{off} values of at least two different materials. In the perfect case, red, green and blue colours could be recognized by selecting three different materials with cut-off wavelengths in three different regions of the optical spectrum: one material that responds only to the blue light ($405\ nm < \lambda_{cut\text{-}off} < 532\ nm$), one that responds to the blue and green light ($532\ nm < \lambda_{cut\text{-}off} < 660\ nm$), and one that responds to all three ($\lambda_{cut\text{-}off} > 660\ nm$); and by illuminating them simultaneously with the same light and comparing all photoresponse signals. However, in our case, only ZnSe measurement solely determined the incident (blue) light due to its cut-off wavelength. Other studied materials exhibited substantial decrease in photoresponse in respect of the increasing wavelength, but still significant response was measured for the light with the longest wavelength, presumably due to some defect states, such as NW surface, or impurity doping. Thus, in such instance, one can only distinguish red and green or blue and green light of the same intensity by comparing absolute I_{on}/I_{off} values of, for example, PbS and CdS. Comparison could be made through logic operations of the

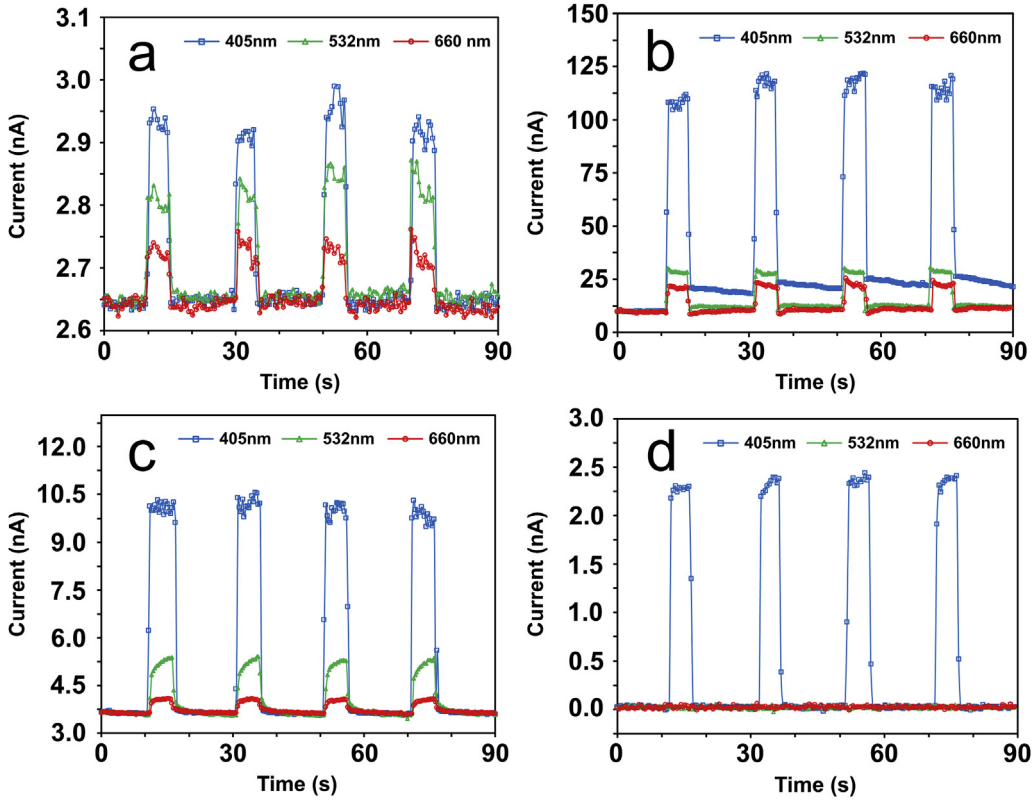

Fig. 6. On-off photoresponse measurements of (a) PbS, (b) In_2S_3, (c) CdS and (d) ZnSe nanowire photoresistors at V_{ds} = 1 V bias voltage and 2 W/cm^2 light intensity of 405 nm, 532 nm and 660 nm wavelength light illumination. The diameters of PbS, In_2S_3, CdS and ZnSe NWs are 120, 160, 180 and 280 nm, respectively.

Table 1
Comparison of the photoresponses of the studied nanowire-based photoresistors.

Materials	E_g (eV)	I_{dark} at 1 V (nA)	I_{on}/I_{off} ratio		
			at 405 nm (3.06 eV)	at 532 nm (2.33 eV)	at 660 nm (1.88 eV)
PbS NW	0.41	2.65	1.11	1.07	1.03
In_2S_3 NW	2.1	9.95	11.3	2.8	2.1
CdS NW	2.4	3.65	2.7	1.4	1.1
ZnSe NW	2.7	0.02	115	1	1

Table 2
Responsivity R_λ and external quantum efficiency EQE values of the studied nanowire-based photoresistors at different illumination wavelengths.

Materials	R_λ, A/W			EQE		
	at 405 nm	at 532 nm	at 660 nm	at 405 nm	at 532 nm	at 660 nm
PbS NW	0.06	0.04	0.02	18%	9%	3%
In_2S_3 NW	16.01	2.80	1.71	4903%	652%	321%
CdS NW	0.86	0.20	0.05	264%	47%	10%
ZnSe NW	0.20	0	0	62%	0	0

specific NW current signals, which arise from distinct photoresponse values of NWs [38,39]. However, this above-cut-off-wavelength photoresponse might be considerably reduced by surface passivation, therefore simplifying the principle of colour distinction. That could be done by producing a shell layer around the core material that eliminates its surface trap states, and could even lead to an enhanced photosensitivity [40–42]. In general, choosing different photosensitive NWs for desired spectral range, depending on the application, is possible yet not always sufficient – defects, such as NW surface, or impurity doping can result in above-cut-off-wavelength photosensitivity.

4. Conclusions

PbS, In_2S_3, CdS and ZnSe NWs were synthesised via atmospheric pressure chemical vapour transport method. Samples were characterized by SEM, TEM methods, XRD technique, which revealed their highly crystalline structure, and PL measurements to investigate their optical properties. Two-terminal photoresistor devices were fabricated from as-grown NWs using *in situ* nanomanipulations and electron-beam-assisted Pt deposition inside SEM-FIB; their current-voltage and photoresponse measurements were performed under the same conditions. Two approaches for

determining the colour (red, green or blue) with as-prepared NW photoresistors were discussed. While determination via the cut-off wavelength due to the bandgap would be the best approach in this case, considerable above-cut-off-wavelength photosensitivity was observed; therefore, a method for reducing this undesired photoresponse is necessary to be implemented.

Acknowledgements

Financial support provided by Scientific Research Project for Students and Young Researchers Nr. SJZ/2016/6 realized at the Institute of Solid State Physics, University of Latvia is greatly acknowledged. Authors are grateful to Reinis Ignatans for XRD measurements.

References

[1] E.H. Steenbergen, M.J. DiNezza, W.H.G. Dettlaff, S.H. Lim, Y.-H. Zhang, Optically-addressed two-terminal multicolor photodetector, Appl. Phys. Lett. 97 (2010) 161111, https://doi.org/10.1063/1.3505137.
[2] G. Konstantatos, E.H. Sargent, Nanostructured materials for photon detection, Nat. Nanotechnol. 5 (2010) 391–400, https://doi.org/10.1038/nnano.2010.78.
[3] Y. Liu, R. Cheng, L. Liao, H. Zhou, J. Bai, G. Liu, L. Liu, Y. Huang, X. Duan, Plasmon resonance enhanced multicolour photodetection by graphene, Nat. Commun. 2 (2011) 579, https://doi.org/10.1038/ncomms1589.
[4] E. Laux, C. Genet, T. Skauli, T.W. Ebbesen, Plasmonic photon sorters for spectral and polarimetric imaging, Nat. Photonics 2 (2008) 161–164, https://doi.org/10.1038/nphoton.2008.1.
[5] C. Soci, A. Zhang, B. Xiang, S.A. Dayeh, D.P.R. Aplin, J. Park, X.Y. Bao, Y.H. Lo, D. Wang, ZnO nanowire UV photodetectors with high internal gain, Nano Lett. 7 (2007) 1003–1009, https://doi.org/10.1021/nl070111x.
[6] K. Deng, L. Li, CdS nanoscale photodetectors, Adv. Mater. 26 (2014) 2619–2635, https://doi.org/10.1002/adma.201304621.
[7] R. Graham, C. Miller, E. Oh, D. Yu, Electric field dependent photocurrent decay length in single lead sulfide nanowire field effect transistors, Nano Lett. 11 (2011) 717–722, https://doi.org/10.1021/nl1038456.
[8] X. Xie, G. Shen, Single-crystalline In2S3 nanowire-based flexible visible-light photodetectors with an ultra-high photoresponse, Nanoscale 7 (2015) 5046–5052, https://doi.org/10.1039/C5NR00410A.
[9] C.H. Hsiao, S.J. Chang, S.B. Wang, S.P. Chang, T.C. Li, W.J. Lin, C.H. Ko, T.M. Kuan, B.R. Huang, ZnSe nanowire photodetector prepared on oxidized silicon substrate by molecular-beam epitaxy, J. Electrochem. Soc. 156 (2009), https://doi.org/10.1149/1.3077580. J73.
[10] T. Takahashi, P. Nichols, K. Takei, A.C. Ford, A. Jamshidi, M.C. Wu, C.Z. Ning, A. Javey, Contact printing of compositionally graded CdSxSe1-x nanowire parallel arrays for tunable photodetectors, Nanotechnology 23 (2012) 45201, https://doi.org/10.1088/0957-4484/23/4/045201.
[11] H. Dedong, L. Ying-Kai, D. Yu, Multicolor photodetector of a single Er3+-Doped CdS nanoribbon, Nanoscale Res. Lett. 10 (2015) 285, https://doi.org/10.1186/s11671-015-0975-3.
[12] H. Park, Y. Dan, K. Seo, Y.J. Yu, P.K. Duane, M. Wober, K.B. Crozier, Filter-free image sensor pixels comprising silicon nanowires with selective color absorption, Nano Lett. 14 (2014) 1804–1809, https://doi.org/10.1021/nl404379w.
[13] X. Liu, L. Jiang, X. Zou, X. Xiao, S. Guo, C. Jiang, X. Liu, Z. Fan, W. Hu, X. Chen, W. Lu, W. Hu, L. Liao, Scalable integration of indium zinc oxide/photosensitive-nanowire composite thin-film transistors for transparent multicolor photodetectors array, Adv. Mater. 26 (2014) 2919–2924, https://doi.org/10.1002/adma.201305073.
[14] L. Sang, J. Hu, R. Zou, Y. Koide, M. Liao, Arbitrary multicolor photodetection by hetero-integrated semiconductor nanostructures, Sci. Rep. 3 (2013) 2368, https://doi.org/10.1038/srep02368.
[15] Z. Fan, J.C. Ho, T. Takahashi, R. Yerushalmi, K. Takei, A.C. Ford, Y.-L. Chueh, A. Javey, Toward the development of printable nanowire electronics and sensors, Adv. Mater. 21 (2009) 3730–3743, https://doi.org/10.1002/adma.200900860.
[16] S.Y. Jang, Y.M. Song, H.S. Kim, Y.J. Cho, Y.S. Seo, G.B. Jung, C. Lee, J. Park, M. Jung, J. Kim, B. Kim, J.-G. Kim, Y.-J. Kim, Three synthetic routes to single-crystalline PbS nanowires with controlled growth direction and their electrical transport properties, ACS Nano 4 (2010) 2391–2401, https://doi.org/10.1021/nn100163k.
[17] M. Zervos, P. Papageorgiou, A. Othonos, High yield–low temperature growth of indium sulphide nanowires via chemical vapor deposition, J. Cryst. Growth 312 (2010) 656–661, https://doi.org/10.1016/j.jcrysgro.2009.12.023.
[18] Y. Wang, G. Meng, L. Zhang, C. Liang, J. Zhang, Catalytic growth of large-scale single-crystal CdS nanowires by physical evaporation and their photoluminescence, Chem. Mater. 14 (2002) 1773–1777, https://doi.org/10.1021/cm0115564.
[19] U. Philipose, P. Sun, T. Xu, H.E. Ruda, L. Yang, K.L. Kavanagh, Structure and photoluminescence of ZnSe nanostructures fabricated by vapor phase growth, J. Appl. Phys. 101 (2007) 14326, https://doi.org/10.1063/1.2424400.
[20] A. Datta, G. Sinha, S.K. Panda, A. Patra, Growth, optical, and electrical properties of In2S3 zigzag nanowires, Cryst. Growth Des. 9 (2009) 427–431, https://doi.org/10.1021/cg800663t.
[21] L. Dong, J. Jiao, M. Coulter, L. Love, Catalytic growth of CdS nanobelts and nanowires on tungsten substrates, Chem. Phys. Lett. 376 (2003) 653–658, https://doi.org/10.1016/S0009-2614(03)01059-5.
[22] S. Kar, S. Biswas, S. Chaudhuri, Catalytic growth and photoluminescence properties of ZnS nanowires, Nanotechnology 16 (2005) 737–740, https://doi.org/10.1088/0957-4484/16/6/018.
[23] Y.K. Albert Lau, D.J. Chernak, M.J. Bierman, S. Jin, Epitaxial growth of hierarchical PbS nanowires, J. Mater. Chem. 19 (2009) 934, https://doi.org/10.1039/b818187j.
[24] JCPDS Card No. 78–1058, (n.d.).
[25] JCPDS Card No. 25–0390, (n.d.).
[26] JCPDS Card No. 21–829, (n.d.).
[27] JCPDS Card No. 37–1463, (n.d.).
[28] JCPDS Card No. 41–1049, (n.d.).
[29] N.S. Dantas, A.F. da Silva, C. Persson, Electronic band-edge properties of rock salt PbY and SnY (Y= S, Se, and Te), Opt. Mater. (Amst) 30 (2008) 1451–1460, https://doi.org/10.1016/j.optmat.2007.09.001.
[30] A.D. Andreev, A.A. Lipovskii, Anisotropy-induced optical transitions in PbSe and PbS spherical quantum dots, Phys. Rev. B 59 (1999) 15402–15404, https://doi.org/10.1103/PhysRevB.59.15402.
[31] H. Cao, G. Wang, S. Zhang, X. Zhang, Growth and photoluminescence properties of PbS nanocubes, Nanotechnology 17 (2006) 3280–3287, https://doi.org/10.1088/0957-4484/17/13/034.
[32] T. Tohidi, K. Jamshidi-Ghaleh, Optical and structural properties of nanocrystalline PbS thin film grown by CBD on Si(1 0 0) substrate, Philos. Mag. 94 (2014) 3368–3381, https://doi.org/10.1080/14786435.2014.959579.
[33] A.A. Talin, F. Léonard, B.S. Swartzentruber, X. Wang, S.D. Hersee, Unusually strong space-charge-limited current in thin wires, Phys. Rev. Lett. 101 (2008) 76802, https://doi.org/10.1103/PhysRevLett.101.076802.
[34] A.M. Katzenmeyer, F. Leonard, A.A. Talin, M.E. Toimil-Molares, J.G. Cederberg, J.Y. Huang, J.L. Lensch-Falk, Observation of space-charge-limited transport in InAs nanowires, IEEE Trans. Nanotechnol. 10 (2011) 92–95, https://doi.org/10.1109/TNANO.2010.2062198.
[35] A. Vilà, F. Hernández-Ramirez, J. Rodríguez, O. Casals, A. Romano-Rodríguez, J.R. Morante, M. Abid, Fabrication of metallic contacts to nanometre-sized materials using a focused ion beam (FIB), Mater. Sci. Eng. C 26 (2006) 1063–1066, https://doi.org/10.1016/j.msec.2005.09.092.
[36] Y. Ye, L. Dai, X. Wen, P. Wu, R. Pen, G. Qin, High-performance single CdS nanobelt metal-semiconductor field-effect transistor-based photodetectors, ACS Appl. Mater. Interfaces 2 (2010) 2724–2727, https://doi.org/10.1021/am100661x.
[37] T. Zhai, L. Li, X. Wang, X. Fang, Y. Bando, D. Golberg, Recent developments in one-dimensional inorganic nanostructures for photodetectors, Adv. Funct. Mater. 20 (2010) 4233–4248, https://doi.org/10.1002/adfm.201001259.
[38] Y.-Q. Bie, Z.-M. Liao, H.-Z. Zhang, G.-R. Li, Y. Ye, Y.-B. Zhou, J. Xu, Z.-X. Qin, L. Dai, D.-P. Yu, Self-powered, ultrafast, visible-blind UV detection and optical logical operation based on ZnO/GaN nanoscale p-n junctions, Adv. Mater. 23 (2011) 649–653, https://doi.org/10.1002/adma.201003156.
[39] Z. Fan, J.C. Ho, Z.A. Jacobson, H. Razavi, A. Javey, Large-scale, heterogeneous integration of nanowire arrays for image sensor circuitry, Proc. Natl. Acad. Sci. 105 (2008) 11066–11070, https://doi.org/10.1073/pnas.0801994105.
[40] L. Qin, C. Shing, S. Sawyer, P.S. Dutta, Enhanced ultraviolet sensitivity of zinc oxide nanoparticle photoconductors by surface passivation, Opt. Mater. (Amst) 33 (2011) 359–362, https://doi.org/10.1016/j.optmat.2010.09.020.
[41] K. Moazzami, T.E. Murphy, J.D. Phillips, M.C.-K. Cheung, A.N. Cartwright, Sub-bandgap photoconductivity in ZnO epilayers and extraction of trap density spectra, Semicond. Sci. Technol. 21 (2006) 717–723, https://doi.org/10.1088/0268-1242/21/6/001.
[42] Y. Dan, K. Seo, K. Takei, J.H. Meza, A. Javey, K.B. Crozier, Dramatic reduction of surface recombination by in situ surface passivation of silicon nanowires, Nano Lett. 11 (2011) 2527–2532, https://doi.org/10.1021/nl201179n.